STRENGTH OF COMPOSITE SANDWICH PANELS CONTAINING DEBONDS

W. C. KIM, T. C. MILLER† and C. K. H. DHARAN

Department of Mechanical Engineering, University of California, Berkeley, CA 94720, U.S.A.

Abstract—A method for determining the critical debond size between the facesheet and the core in composite sandwich panels under in-plane compression is described. The approach uses fracture mechanics together with a buckling criterion for a debonded faceskin. The technique yields predictions for the critical in-plane compressive load for debond propagation as a function of core-to-faceskin debond size, faceskin thickness, lay-up, composite material properties, and honeycomb properties and geometries. A computer program, developed in this work, calculates the critical buckling load and facesheet deformed shape by solving an eigenvalue problem. An experimental study was conducted to determine the onset of delamination buckling in composite sandwich panels containing such flaws. Sandwich panel specimens of graphite/epoxy faceskins and aluminum honeycomb core were constructed with embedded delaminations and with varying faceskin thicknesses and core sizes. Four-point bending tests were conducted such that the faceskin containing the debond was under in-plane compression. The predicted critical fracture loads, computed using the proposed theoretical models which were solved using a numerical computational scheme, closely followed the experimental measurements.

INTRODUCTION

Delamination in composite laminates has received considerable attention recently, since it is the preferred crack propagation mode in such structures. Delamination often initiates from defects which arise from local impact damage and manufacturing flaws. One important flow is ply debonding due to poor local adhesion or to the presence of interlaminar contaminants.

There have been several studies conducted on delamination buckling induced by in-plane compression in composite laminates. General analyses on the subject are mainly associated with a static buckling analysis of a pre-existing delaminated sublaminate. Linear elastic fracture mechanics (LEFM) has also been used successfully to predict fracture behavior in composite laminates, especially delamination fracture (Dharan, 1978; Kim and Dharan, 1989). These studies were conducted by either a finite element method (FEM) or an application of a beam/plate theory such as von Karman's nonlinear plate theory. Chai and Babcock (1985) analysed buckling of a close-to-the-surface delaminated elliptical layer using the Rayleigh–Ritz method. Buckling of a thin sublaminate in a quasi-isotropic composite was also studied using FEM by Shivakumar and Whitcomb (1985). Von Karman's plate theory was applied to delamination buckling of a two-layer axisymmetric model of a circular plate with an initial penny-shaped delamination (Bottega and Maewal, 1983).

The major theoretical conclusions of these studies on delamination growth under axial compression are (Bruno and Grimaldi, 1990; Whitcomb, 1989; Kachanov, 1988; Chai, 1986; Shivakumar and Whitcomb, 1985; Bottega and Maewal, 1983):

(1) The stress at the debond crack tip promotes further splitting only after buckling has occurred. In fact, only in this case is the energy release rate positive. Therefore, the question of debond growth is of interest only for $P \geqslant (P_{cr})_{\text{buckling}}$.
(2) Although there exist, in general, three kinds of fracture modes (Mode I, Mode II and Mode III), debond growth in the present case is expected to be dominated by the interlaminar normal stress so that Mode I fracture is the primary mechanism for debond growth.

---

† Present address: Systron Donner, 2731 Systron Drive, Concord, CA 94518, U.S.A.

Initial debonding

Honeycomb core   Composite faceskin

(a)

Buckled subliminate

P P

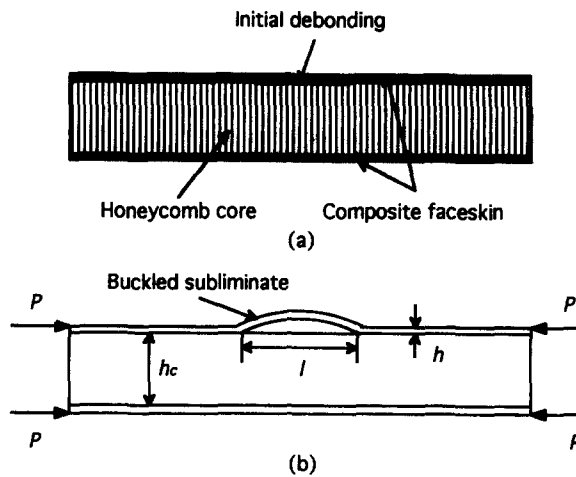h_c l h

P P

(b)

Fig. 1. (a) A sandwich panel with an initial debond between core and faceskin, and (b) its buckled shape.

(3) It is more convenient to use the path independent integral, J, for debond growth, since the computation of J is conducted by calculating a strain energy balance of the system without requiring a consideration of each stress state.

Debonding in composite sandwich honeycomb panels is similar to delamination in laminates and can be approached in a like fashion. In sandwich panels, debonding can be present initially in the form of adhesive film defects, insufficient or uneven pressure on the faceskins during cure, etc. When the sandwich panel is subjected to in-plane compression or bending such that the faceskin containing the defect is in compression, the debond can propagate in a manner analogous to compression-induced delamination buckling and propagation in laminates (Fig. 1). The result is catastrophic failure. Other possible failure modes may consist of failure through the core, adhesive failure, and cohesive failure within the faceskin. The only difference between delamination buckling in composite laminates and in sandwich structures is the role of the core on debond growth in sandwich panels. In theory, the core should also store some amount of strain energy as buckling occurs and propagates.

A model developed by Vizzini and Lagace (1987) is a feasible approach for addressing the current problem of the growth of the debond between the core and the faceskin in a composite sandwich panel. In the model, they considered the effect of a thin matrix layer between plies, modeled as an elastic foundation, to compute the critical static buckling load per unit width of a composite sublaminate subjected to an axial compressive load.

Incorporation of the static analysis derived from this model together with LEFM could be used to predict the critical debond length for a given compressive load in sandwich panels. One can, therefore, model the composite faceskin as a beam or plate resting on an elastic foundation (the core) which imposes reaction forces on the faceskin. This approach makes the model applicable to less rigid cores such as low-density aluminum honeycomb and foam cores. It is also believed to be a more realistic model of the actual problem in which the core and the adhesive account for some of the strain energy in the process of buckling and propagation of the sublaminate.

This paper, therefore, describes an approach that employs LEFM to determine the critical in-plane compressive load for propagation of an initial debond between the faceskin and honeycomb core in a sandwich panel (Fig. 1). As an introductory and rule-of-thumb design concept, the solution of a simple delamination buckling and propagation problem is presented together with a more refined analysis. A method for estimating the fracture energy release rate as a function of core geometry is also proposed and incorporated into the analysis. A computer program containing all these features was written to enable the designer to specify the allowable in-plane compressive load for a given detectable debond

size. Experimental verification was obtained by running several tests on sandwich panel specimens with pre-existing flaws. It is suggested that this approach be incorporated into a comprehensive fracture control plan for composite structures (Kim and Dharan, 1989).

ANALYSIS

A static buckling solution of a structure can be obtained in several ways (Euler buckling theory, energy methods such as the Rayleigh–Ritz method, Galerkin's method, etc.). Since a combined approach of the static buckling analysis and LEFM is proposed, it is more pertinent to use the energy method for the static buckling problem. For the prediction of debond growth using classical LEFM, the criterion for stable crack growth is given by

$$J = J_c, \tag{1}$$

where J is the strain energy release rate and J_c the critical strain energy release rate obtainable from a Mode I fracture test of a specific material and geometry. The strain energy release rate is also defined by

$$J = -\frac{\partial \Pi}{\partial l}, \tag{2}$$

where Π is the total potential energy of the system and l is the debond length.

Figure 1(b) describes a sandwich panel in in-plane compression with an initial through-thickness debond. Its one-dimensional representation has geometry and loading that is invariant along the coordinate normal to the plane of the figure.

Two approaches were employed here; the first, called the simple delamination buckling (SDB) model, uses the classical buckling approach for the sublaminate, while the second, called the refined delamination buckling (RDB) model, uses the beam-on-an-elastic-foundation approach, to take into account the compliance of the core, and the Rayleigh–Ritz method. The solution scheme for both models is identical; the analysis of the SDB model is presented first since it provides a direction for solution using the RDB model which requires more computational effort.

It is assumed in both models that initial debonding under in-plane compression grows only after buckling occurs; as mentioned earlier, one might address the problem by using postbuckling analysis with the large deflection assumption. If the deflection is relatively small at the onset of debond growth, however, one can assume that the deflected shape of the sublaminate in the postbuckling process is analogous to the shape in the initial critical buckling state. With this assumption, the membrane energy of the sublaminate, which should be included in the large deflection analysis, is small and can be neglected.

The main strain energy component is the one due to bending for the SDB model, i.e. it is assumed that the only element that is significant for the energy balance is the buckled sublaminate. Similarly, in addition to the bending energy, one can also include the strain energy in the core for the RDB model. A brief discussion of the models proposed and analyses of the corresponding delamination buckling problems, i.e. the relationship between the critical in-plane compressive load and the critical debond length, follow.

The simple delamination buckling (SDB) model

Debond growth in a sandwich panel under in-plane compression is presented in Fig. 2(a), where the debonded sublaminate is shown schematically by a buckled strip with clamped-clamped boundary conditions. As mentioned earlier, the buckled strip is the only significant energy element to be used for computing the total potential energy leading to the value of J in eqn (2).

Deflection of the debonded strip for clamped-clamped boundary conditions is assumed to be
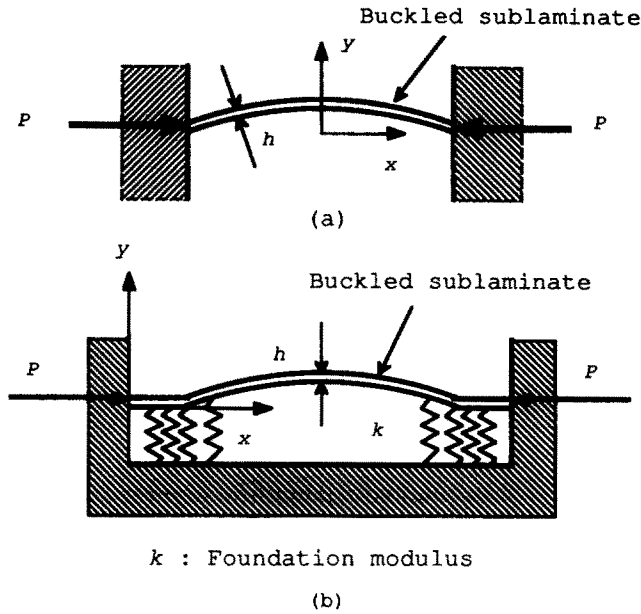
Fig. 2. Two delamination buckling models. (a) The simple delamination buckling (SDB) model, (b) the refined delamination buckling (RDB) model.

$$y(x) = \tfrac{1}{2}A_0\left(1+\cos\frac{2\pi x}{l}\right), \tag{3}$$

where A_0 is the deflection at $x = 0$. The value of A_0 is determined by the condition that the length of the strip, l, does not change in buckling. The contraction due to bending (in buckling) is

$$\Delta l_b = \frac{1}{2}\int_{-l/2}^{l/2}\left(\frac{\mathrm{d}y}{\mathrm{d}x}\right)^2 \mathrm{d}x = \frac{A_0\pi^2}{4l}, \tag{4}$$

whereas the contraction due to the compression stress (before buckling) is

$$\Delta l_c = \varepsilon l = \frac{\sigma}{E_f}\,l, \tag{5}$$

where E_f is the axial Young's modulus of the strip of the faceskin and ε the compressive strain. Equating $\Delta l_b = \Delta l_c$, one obtains

$$A_0^2 = \frac{4\sigma l^2}{E_f\pi^2}. \tag{6}$$

The potential energy of the system is the strain energy due to bending in the strip minus the work done by the applied load at the ends, i.e.

$$\Pi = U_b - W, \tag{7}$$

where

$$U_b = \tfrac{1}{2}E_f I \int_{-1/2}^{1/2} \left(\frac{dy}{dx}\right)^2 dx = \frac{\pi^2 \sigma}{3l} h^3,$$

(8)

$$W = P\Delta l_c = \sigma h \Delta l_c = \frac{l\sigma^2}{E_f} h.$$

(9)

U_b is the bending energy per unit width of the strip and W is the work done by the applied load at the ends. From eqn (1), and eqn (2), the criterion for stable debond growth becomes,

$$J = -\frac{\partial \Pi}{\partial l} = \sigma h \left(\frac{\sigma}{E_f} + \frac{\pi^2}{3}\left(\frac{h}{l}\right)^2 \right) = J_c.$$

(10)

Setting $\sigma = \sigma_c$ with $J = J_c$, the critical load per unit width of the strip for the debond growth, P_{cr}, in terms of the critical debond length, l_c, is given by

$$P_{cr} = h\sigma_c = \frac{h}{2}\left(\left(\frac{E_f^2 \pi^4}{9}\left(\frac{h}{l_c}\right)^4 + 4\frac{E_f}{h}J_c \right)^{1/2} + \frac{\pi^2 E_f}{3}\left(\frac{h}{l_c}\right)^2 \right).$$

(11)

The refined delamination buckling (RDB) model

Inclusion of the core is done by the beam-on-an-elastic foundation model shown in Fig. 2(b). The solution method is the same as described earlier. To compute the total potential energy, the core is included in the energy balance of the system; also, the buckling load and shape are determined by the Rayleigh–Ritz energy method. The amplitudes of the assumed deflection functions as a function of a given in-plane compressive load, are obtained as solutions of a linear eigenvalue problem typical of the Rayleigh–Ritz method. The criterion for debond growth using LEFM results in the relationship between the critical fracture load and the corresponding debond length. For a complete solution method for the static buckling problem of a beam-on-an-elastic-foundation, the reader is referred to the Appendix.

The deflected shape is written as a Fourier series:

$$y(x) = \sum_{n=1}^{\infty} A_n \phi_n(x),$$

(12)

where $\phi_n(x) = \cos\left(2(n-1)\pi x/l\right) - \cos\left(2n\pi x/l\right)$ is the shape function for clamped-clamped boundary conditions, and A_n are the amplitudes of the individual modes. Using a non-dimensional parameter defined by $\xi = x/l$, the potential energy associated with buckling is given by

$$\Pi = U_b + U_c - W,$$

(13)

with

$$U_b = \frac{E_f I}{2l^3} \int_0^1 \left(\frac{d^2 y}{d\xi^2}\right) d\xi,$$

(14)

$$U_c = \frac{kl}{2} \int_0^1 \psi(\xi) y^2 \, d\xi,$$

(15)

$$W = \frac{P}{2l} \int_0^1 \left(\frac{dy}{d\xi}\right)^2 d\xi,$$

(16)

where U_b is the bending energy, U_c is the strain energy from the foundation (core), W is the work done by the applied load. The function $\psi(\xi)$ is defined in the Appendix.

The critical in-plane load per unit width in terms of the critical debond length is given by

$$J = -\frac{\partial}{\partial l}\left(\frac{E_f I}{2l^3}\alpha + \frac{kl}{2}\beta - \frac{P}{2l}\gamma\right) = J_c, \tag{17}$$

resulting in

$$P_{cr} = \frac{3E_f I\alpha - l_c^4 k\beta - 2l_c^4 J_c}{l_c^2 \gamma}, \tag{18}$$

where

$$I = \frac{h^3}{12}, \tag{19}$$

$$\alpha = \mathbf{A}\int_0^1 \mathbf{\Phi}_2\mathbf{\Phi}_2^T\,d\xi\,\mathbf{A}^T, \tag{20}$$

$$\beta = \mathbf{A}\int_0^1 \psi\mathbf{\Phi}_0\mathbf{\Phi}_0^T\,d\xi\,\mathbf{A}^T, \tag{21}$$

$$\gamma = \mathbf{A}\int_0^1 \mathbf{\Phi}_1\mathbf{\Phi}_1^T\,d\xi\,\mathbf{A}^T. \tag{22}$$

For the definitions of the matrices $\mathbf{A}$, $\mathbf{\Phi}_0$, etc., see the Appendix. One notes that the expression for J in eqn (17) is a more general form of the energy release rate expression since it takes into account dissimilar materials (the faceskin and the core in this case), in which the compliance of each phase must be included.

The elastic modulus of the faceskin, E_f, can be derived from classical laminated plate theory for a given composite material and lay-up. The mechanical properties of the honeycomb core are usually modeled as *effective* properties, which are properties associated with the corresponding homogeneous material. These *effective* properties are functions of the core material properties and geometry, such as the core Young's modulus, E_c, the cell wall thickness, t_c, and cell size, d. For example, the *effective* Young's modulus of a honeycomb core, E_c^e, is often defined as (MIL-HDBK-23, 1988 ; Hexcel Inc., 1984)

$$E_c^e = \frac{8}{3}\frac{t_c}{d}E_c. \tag{23}$$

The geometry of the honeycomb core can be included in the expression for k in eqn (17) such that J is also a function of core geometry, i.e.

$$k = \frac{E_c^e b}{h_c} = \frac{8}{3}\frac{t_c}{dh_c}E_c, \tag{24}$$

where h_c is the height of the core, and b the width of the strip. Mechanical properties of sandwich facings and honeycomb materials can be obtained from the literature, such as MIL-HDBK-23 (1988). Thus, given the geometry and properties of the faceskin and core, eqns (18) and (24) enable the designer to obtain the critical load, P_{cr}, for debond growth as a function of the critical debond length, l_c, provided that the value of J_c for the material system and geometry concerned is available.

Table 1. Specimen characteristics

Core size (mm)	No. of plies	Crack length (mm)
3.2, 4.8	2	0.5, 1.0, 1.5
3.2, 4.8	3	0.75, 1.25, 1.75
3.2, 4.8	4	1.0, 1.5, 2.0

EXPERIMENTAL VERIFICATION

Sandwich panels were constructed with Fiberite's graphite/epoxy prepreg consisting of woven T-300 graphite fibers in 934 epoxy matrix, and laminated into the faceskins which were bonded to aluminum honeycomb cores. Specimen dimensions (44 mm width and 280 mm length) were selected to ensure that the faceskins buckled and delaminated before the failure strength of the faceskins. The initial debonds were produced by applying Teflon tape between the upper faceskin and the core across the entire width of the specimens before bonding of the faceskins. A total of 18 sandwich panels were fabricated and tested to determine the critical fracture loads. Six batches of three specimens were fabricated for each combination of the two different core geometries and three faceskin thicknesses (see Table 1).

The graphite/epoxy faceskins, manufactured from 2, 3 and 4 layers of 0.3 mm thick preimpregnated plain weave cloth, were cured according to the manufacturer's cure schedule in a microprocessor-controlled heated platen press. All plies were oriented in a 0°/90° configuration with respect to the axis of the panels. The surface of each faceskin (the surface exposed to the blotter) was sanded lightly with 400 grit sandpaper and cleaned with solvent.

After applying 0.025 mm thick Teflon tape to simulate a debond, the core and faceskins were bonded with one layer of Ciba-Giegy film adhesive using a vacuum bag and heating the assembly to 177°C. Two aluminum core materials were used: 25.4 mm thick, 3/16-5052-0.0008 and 12.7 mm thick, 1/8-5052-0.002 hexagonal aluminum honeycomb (4.8 mm and 3.2 mm cell sizes, respectively) and were oriented with the ribbon direction along the length of the specimens. A single strain gage (Micro Measurements CEA-06-250VW-350) was applied to the critical faceskin between the debond and one loading point to measure the corresponding in-plane strain as shown in Fig. 3. The specimen characteristics are given in Table 1.

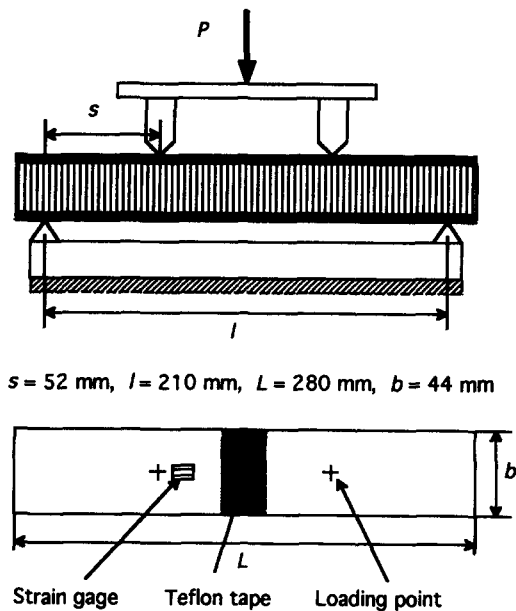$s = 52$ mm, $l = 210$ mm, $L = 280$ mm, $b = 44$ mm

Fig. 3. Four point bending fixture and a typical graphite/epoxy faceskin with a strain gage.
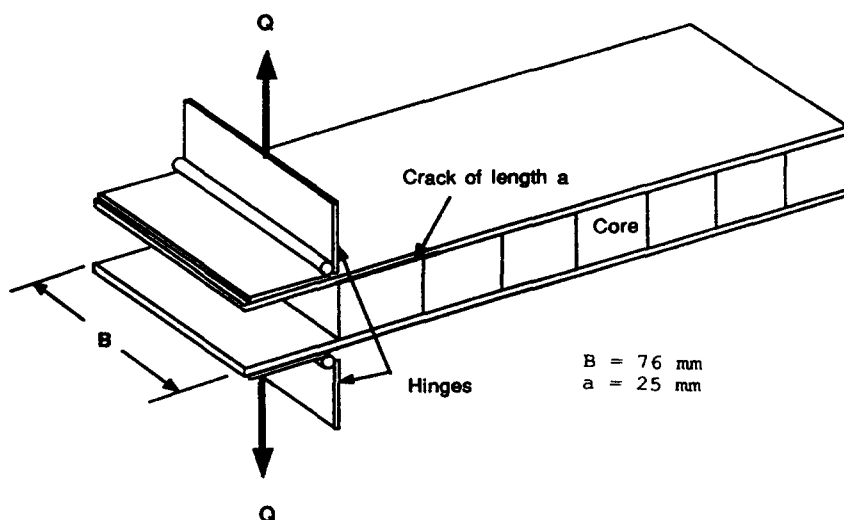
Fig. 4. Fracture toughness specimen.

To utilize eqns (11) and (18) for computing the critical fracture load, a measure of J_c is necessary. Together with the specimens for the debonding test, therefore, fracture specimens (152 mm long by 76 mm wide) were fabricated to measure the J_c values. These specimens were constructed with three plies of the graphite/epoxy faceskin and two different core sizes (4.8 mm and 3.2 mm cell sizes). A 6061 aluminum plate (3 mm thick) was bonded with film adhesive to each faceskin to ensure that the Mode I loading condition is met. Figure 4 shows a sketch of the fracture specimen.

The testing configuration employed for measuring J_c is not pure Mode I due to the stiffness difference between the two deflected parts of the specimen. However, the difference in stiffness is small since the core has high compliance once it is separated from the facesheet by crack propagation. It was assumed that the test procedure for obtaining G_{Ic} can be successfully applied to the current fracture toughness test (Carlsson and Pipes, 1989). The dominant fracture mechanism has been shown to be Mode I for the delamination buckling fracture of composite laminates by a number of investigators (Shivakumar and Whitcomb, 1985; Whitcomb, 1989; Bruno and Grimaldi, 1990).

Keeping this assumption in mind, J_c can be determined using the following relation :

$$J_c \cong G_{Ic} = \frac{Q^2}{2B} \frac{dC}{da} = \frac{Q^2}{2B} \frac{a^2}{EI}, \tag{25}$$

where Q represents the load at fracture, a is the crack length, B the width, C the compliance, and EI is the product of modulus and inertia for the aluminum/graphite laminate. The experimental results are presented in Table 2.

The SDB and RDB models for the critical delamination load were verified using four point bending. This loading was selected since it reduces the possibility of unequal loading of the facesheets, a condition which tends to occur in in-plane compression testing due to specimen misalignment (Pearce and Webber, 1972). Faceskin bending was assumed to be negligible during testing because of the small faceskin thickness/core thickness ratio.

Table 2. Measured fracture toughness values

Core size (mm)	$P_{cr}(N)$	J_c (N m^{-1})
3.2	165	5.4
4.8	147	4.4

A servohydraulic testing machine (MTS), using specially constructed loading noses to minimize local loading of the core, was used to load each specimen. Figure 3 shows the experimental arrangement. The load was applied using an MTS controller with a generated ramp signal of 0.254 mm s^{-1}. The strain gage reading was conditioned with a Measurements Group amplifier/conditioner 2110/2120, and the output signal from these instruments was plotted on a strip chart recorder (Gould Brush 260). In addition to strain gage measurements, the applied force versus load displacement plot was obtained using an x–y recorder. The slope of the plot was used to determine the effective thickness of the graphite/epoxy faceskin, h, using the following relation derived from beam theory:

$$\frac{\Delta}{F} = \frac{s^2}{6E_f I}(s + \tfrac{3}{2}l) \quad \text{with} \quad I \cong \frac{bht_c^2}{2}, \tag{26}$$

where s and l are distances between loading points in the four-point test fixture, as shown in Fig. 3, and Δ is the deflection of the mid-point of the specimen. The faceskin modulus, calculated from laminated plate theory, was 66 GPa. Direct measurements of h with a micrometer were found to be prone to error because of the uneven texture of the graphite fiber weave.

For some specimens requiring high in-plane loads (small debonds and/or thick faceskins), core shear failure was the dominant failure mode rather than delamination propagation. Consequently, these specimens had to be altered to allow direct compression on the MTS machine. This was achieved by shortening the sample lengths to approximately 127 mm and milling the ends square. Despite these efforts, only 15 of the 18 sandwich panels produced useful data. The remaining three specimens exhibited overall buckling before delaminating and were discarded.

A Fortran program that computes the critical fracture loads in terms of the critical debond length for the two models was written. An initial critical debond length of 2.5 mm was chosen and increased by 2.5 mm in each iteration to compute the critical fracture load up to 51 mm. The initial debond length for the program was chosen since a preliminary analysis of the current problem showed premature failure by yielding of the faceskin material for low initial debond length. An experimental finding for this argument was presented by Harris and Nordby (1969) who conducted debonding tests using 6 mm thick faceskins of Douglas fir plywood over a 76 mm thick foam core. From these test results, in which a simple static buckling analysis was used, a 51 mm long debond did not affect the failure stress, while the 102 mm debond reduced the failure stress only slightly. Thus, there appears to exist a limit for the minimum debond length that can propagate (as predicted
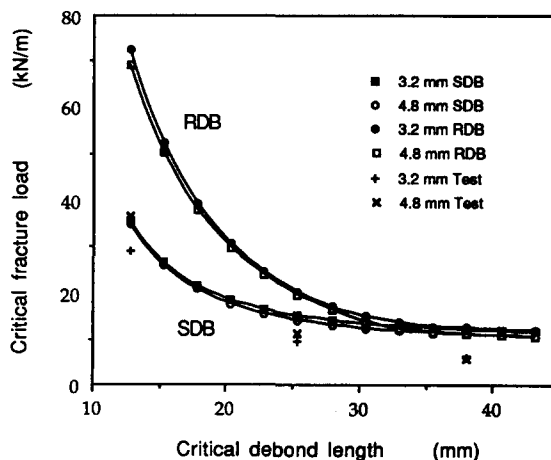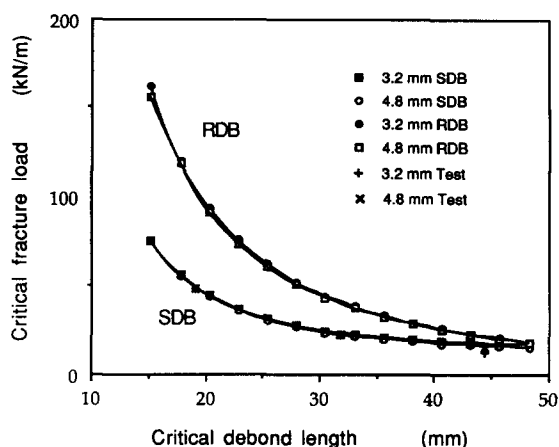

Fig. 5. Predicted critical fracture load vs critical debond length and test results for 2-ply graphite/epoxy sandwich panels with two different core sizes. Note that the RDB model approaches the SDB model when the core contribution is small. This is the case for the specimens tested which had low J_c values.

Fig. 6. Predicted critical fracture load vs critical debond length and test results for 3-ply graphite/epoxy sandwich panels with two different core sizes. Note that the RDB model approaches the SDB model when the core contribution is small. This is the case for the specimens tested which had low J_c values.

by LEFM) for debond-intiated buckling failure of a sandwich panel. If a nondestructive evaluation (Kim and Dharan, 1989) of the composite sandwich panel is conducted, debonds below this limit should be analysed by a static theory of failure.

Figures 5–7 show the experimental and predicted curves obtained for each of the three faceskin thicknesses (2, 3 and 4 plies). Figures 5 and 6 show that the measured critical fracture load per unit width is close to the SDB model. However, in Fig. 7, the data for 4-ply faceskins show lower critical fracture loads than predicted, especially for small initial debonds. The experimental data in Figs 5–7 show better correlation with the SDB prediction; this is due to the lower contribution by the core in the specimens that were tested. These specimens were characterized by poor bonding between the faceskins and core which resulted in relatively low values for J_c (see Table 2). One should note that the RDB model, which fully takes into account the contribution by the core, degenerates to the SDB model when the core strain energy is neglected. Thus, the RDB model is more general. For relatively long debonds, the two models are very close in their predictions. For practical design purposes, the SDB model provides a lower bound for the critical fracture load, and is a quick and easy method for obtaining the critical fracture load.
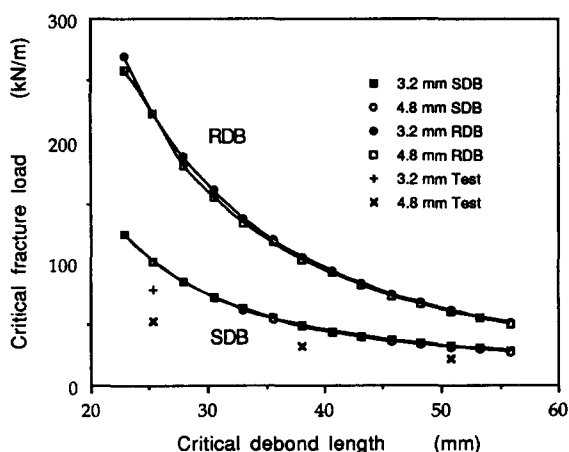

Fig. 7. Predicted critical fracture load vs critical debond length and test results for 4-ply graphite/epoxy sandwich panels with two different core sizes. Note that the RDB model approaches the SDB model when the core contribution is small. This is the case for the specimens tested which had low J_c values.

CONCLUSIONS

It has been shown that buckling analysis and LEFM applied to the problem of debond growth in sandwich panels can predict the critical in-plane compressive load for debond growth in a composite sandwich panel. The two analytical models developed, the SDB and the RDB models, predict almost the same critical fracture load for relatively large initial debonds. Failure of the faceskin itself was the dominant failure mode for small initial debonds under compression. Experimental results employing 2-, 3- and 4-ply woven graphite/epoxy faceskins with four point bending as well as direct compression tests followed closely the theoretical predictions of the critical fracture loads. The design approach proposed here can lead to the damage tolerant design of composite sandwich panels if appropriate techniques for detecting the critical flaw size are used. Useful design criteria for sandwich structures containing initial debonds subjected to in-plane compression can be established and incorporated into a suitable fracture control plan. Furthermore, similar design methodology can be applied to other flaw shapes, such as square and elliptically shaped debonds, and other loading conditions.

REFERENCES

Bottega, W. J. and Maewal, A. (1983). Delamination buckling and growth in laminates. *J. Appl. Mech.* **50**, 184–189.

Bruno, D. and Grimaldi, A. (1990). Delamination failure of layered composite plates loaded in compression. *Int. J. Solids Structures* **26**, 313–330.

Carlsson, L. A. and Pipes, R. B. (1989). *Experimental Characterization of Advanced Composite Materials*. Prentice-Hall, Englewood, NJ.

Chai, H. (1986). On the correlation between the mode I failure of adhesive joints and laminated composites. *Engng Fract. Mech.* **24**, 413–431.

Chai, H. and Babcock, C. D. (1985). Two-dimensional modeling of compressive failure in delaminated laminates. *J. Compos. Mater.* **19**, 67–98.

Dharan, C. K. H. (1978). Fracture mechanics of composite materials. *J. Engng Mater. Technol.* **100**, 233–247.

Harris, J. and Nordby, G. M. (1969). Local failure of plastic-form core sandwich panels. *J. Struct. Div., Proc. ASCE*, 585–601.

Hexcel Inc. (1984). Mechanical Properties of Hexcel Honeycomb Materials. No. TSB 120.

Kachanov, L. M. (1988). *Delamination Buckling of Composite Materials*. Kluwer, Brookline, MA.

Kim, W. C. and Dharan, C. K. H. (1989). A fracture control plan for composite structures. *Engng Fract. Mech.* **34**, 305–324.

MIL-HDBK-23 (1988). U.S. Government Printing Office. Washington, DC.

Pearce, T. R. A. and Webber, J. P. H. (1972). Buckling of sandwich panels with laminated face plates. *Aero. Q.* **23**, 148–160.

Shivakumar, K. N. and Whitcomb, J. D. (1985). Buckling of a sublaminate in a quasi-isotropic composite laminate. *J. Compos. Mater.* **19**, 2–18.

Vizzini, A. J. and Lagace, P. A. (1987). The buckling of a delaminated sublaminate on an elastic foundation. *J. Compos. Mater.* **21**, 1106–1117.

Whitcomb, J. D. (1989). Comparison of full 3-d, thin-film 3-d, and thin-film plate analyses of a postbuckled embedded delamination. *J. Compos. Technol. & Res.* **11**, 154–157.

APPENDIX: SOLUTION OF THE STATIC BUCKLING PROBLEM FOR THE RDB MODEL

This section provides the solution for the static buckling problem of a strip on an elastic foundation used in the RDB model [see Fig. 2(b)]. The assumed deflection function for clamped-clamped boundary conditions is

$$Y(x) = \sum_{n=1}^{\infty} A_n \phi_n(x), \tag{A1}$$

where the shape functions are defined by $\phi_n(x) = \cos[2(n-1)\pi x/l] - \cos[2n\pi x/l]$ and A_n are the amplitudes of the individual modes in a Fourier series. In computer implementation of the deflection function, a specific number (e.g. 20) of the assumed mode shape should be used depending on the computation speed.

The energy expressions which correspond to the bending energy, the strain energy from the foundation, and the work done by the applied load, are as follows:
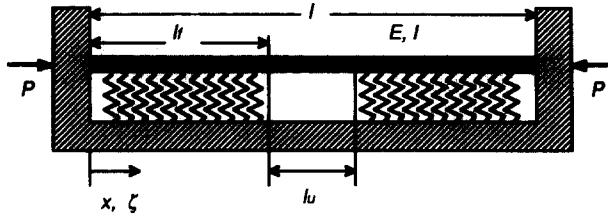
Fig. A1. A strip on an elastic foundation (l = overall length, l_f = foundation length, l_u = unsupported length, h = thickness of the beam, k = spring constant of the foundation per unit length, E = modulus of the beam), (Vizzini and Lagace, 1987).

$$U_b = \frac{E_f I}{2} \int_0^l \left(\frac{d^2 y}{dx^2}\right)^2 dx, \tag{A2}$$

$$U_c = \frac{1}{2} \int_0^l k(x) y^2 \, dx, \tag{A3}$$

$$W = \frac{P}{2} \int_0^l \left(\frac{dy}{dx}\right)^2 dx, \tag{A4}$$

which can be transformed into eqns (14)–(16) using a nondimensional parameter, $\xi = x/l$. The function $\psi(\xi)$ representing a scale factor of the reaction force from the foundation is defined by

$$\psi(\xi) = \begin{cases} 1 & \text{if } 0 \leqslant \xi \leqslant \eta, \\ 0 & \text{if } \eta \leqslant \xi \leqslant 1-\eta, \\ 1 & \text{if } 1-\eta \leqslant \xi \leqslant 1, \end{cases} \tag{A5}$$

where $\eta = l_f/l$ (Fig. A1).

For computer implementation of the equations for the energy components, matrix notation has been used and is given by

$$U_b = \frac{E_f I}{2l^3} \mathbf{A} \int_0^1 \mathbf{\Phi}_2 \mathbf{\Phi}_2^T \, d\xi \, \mathbf{A}^T, \tag{A6}$$

$$U_c = \frac{kl}{2} \mathbf{A} \int_0^1 \psi \mathbf{\Phi}_0 \mathbf{\Phi}_0^T \, d\xi \, \mathbf{A}^T, \tag{A7}$$

$$W = \frac{P}{2l} \mathbf{A} \int_0^1 \mathbf{\Phi}_1 \mathbf{\Phi}_1^T \, d\xi \, \mathbf{A}^T, \tag{A8}$$

where the matrices $\mathbf{A}$, $\mathbf{\Phi}_0$, $\mathbf{\Phi}_1$ and $\mathbf{\Phi}_2$ are defined as

$$\mathbf{A} = [A_1 \; A_2 \; \ldots \; A_n], \tag{A9}$$

$$\mathbf{\Phi}_0 = [\tilde{\phi}_1 \; \tilde{\phi}_2 \; \ldots \; \tilde{\phi}_n]^T, \tag{A10}$$

$$\mathbf{\Phi}_1 = \left[\frac{d\tilde{\phi}_1}{d\xi} \frac{d\tilde{\phi}_2}{d\xi} \cdots \frac{d\tilde{\phi}_n}{d\xi}\right]^T, \tag{A11}$$

$$\mathbf{\Phi}_2 = \left[\frac{d^2\tilde{\phi}_1}{d\xi^2} \frac{d^2\tilde{\phi}_2}{d\xi^2} \cdots \frac{d^2\tilde{\phi}_n}{d\xi^2}\right]^T, \tag{A12}$$

with $\tilde{\phi}_n(\xi) = \cos 2(n-1)\pi\xi - \cos 2n\pi\xi$, and n is the number of the shape functions in the deflection assumption.

Defining the potential energy of the system by $\Pi = U_b + U_c - W$, the use of the theory of minimum potential energy yields a linear eigenvalue problem for obtaining the buckling load and shape of the buckled strip:

$$\frac{\partial \Pi}{\partial \mathbf{A}} = 0 \quad \text{and} \quad \mathbf{SA}^T = \lambda \mathbf{A}^T \quad \text{with} \quad \lambda = \frac{E_f I}{P l^2}. \tag{A13}$$

The definitions of the matrices and other parameters are as follows:

$$\mathbf{S} = \mathbf{R}^{-1} \mathbf{Q}, \tag{A14}$$

with

$$\mathbf{R} = \int_0^1 \mathbf{\Phi}_2 \mathbf{\Phi}_2^T \, d\xi + \frac{kl_u^4}{EI(1-2\eta)^4} \int_0^1 \psi \mathbf{\Phi}_0 \mathbf{\Phi}_0^T \, d\xi, \quad \text{and} \tag{A15}$$

$$\mathbf{Q} = \int_0^1 \mathbf{\Phi}_1 \mathbf{\Phi}_1^T \, d\xi. \tag{A16}$$

The solution of eqn (A13) for the largest eigenvalue, which is a component of the eigenvector $\mathbf{A}$, yields the lowest buckling load and the corresponding deflection from $y(x) = \mathbf{A}\mathbf{\Phi}_0$.